Spectral modeling of meteorites at UV-Vis-NIR wavelengths

Julia Martikainen[a,*], Antti Penttilä[a], Maria Gritsevich[a,b], Hannakaisa Lindqvist[c], Karri Muinonen[a,d]

[a] *Department of Physics, P.O. Box 64 (Gustaf Hällströmin katu 2a), FI-00014 University of Helsinki, Finland*
[b] *Institute of Physics and Technology, Ural Federal University, Mira str. 19, 620002 Ekaterinburg, Russia*
[c] *Finnish Meteorological Institute, Erik Palménin aukio 1, FI-00101 Helsinki, Finland*
[d] *Finnish Geospational Research Institute FGI, National Land Survey of Finland, Geodeetinrinne 2, FI-02430 Masala, Finland*

Abstract

We present a novel simulation framework for assessing the spectral properties of meteorite specimens. The framework utilizes a ray-optics code, which simulates light scattering by Gaussian-random-sphere particles large compared to the wavelength of the incident light and accounts for internal diffuse scatterers. The code uses incoherent input and computes phase matrices by utilizing incoherent scattering matrices. Reflectance spectra are modeled by introducing a combination of olivine, pyroxene, and iron, the most common materials present in meteorites that dominate their spectral features. The complex refractive indices of olivine and iron are obtained from existing databases. The refractive indices of pyroxene are derived using an optimization that utilizes our ray-optics code and the measured spectrum of the material. We demonstrate our approach by applying it on the measured meteorite reflectance spectra obtained with the University of Helsinki integrating-sphere UV-Vis-NIR spectrometer.

Keywords: Asteroids, Meteorites, Reflectance spectroscopy, Light scattering, Spectral modeling

1. Introduction

Every year approximately $3.7 - 7.8 \times 10^7$ kg of extraterrestrial material bombard the Earth's atmosphere [1]. This material mostly consists of small dust particles that fully ablate in the atmosphere. Nevertheless, some of them survive atmospheric entry and reach the ground [2]. These are called meteorites, our free samples of the Solar System.

Asteroids remain mostly the same for the past 4.5 billion years. They provide us information on the origin, evolution, and current state of the Solar System. Meteorites and asteroids can be linked by matching their respective reflectance spectra. However, this is

*Corresponding author
Email address: julia.martikainen@helsinki.fi (Julia Martikainen)

difficult because the spectral features depend strongly on the surface properties [3]. Asteroid surfaces are usually covered with a regolith, which is a layer of loose material, such as dust and rock. On the other hand, meteorites are free of the regolith. To better interpret the spectra, we need to gain more knowledge of the light-scattering physics involved.

The strength of meteorites imposes a selection effect on those meteorites that survive entry into the atmosphere [4]. It is thought that there is also a dependence on the size. Smaller objects are more easily transported out of the asteroid main belt due to the Yarkovsky effect [5] than the large objects. These in turn are from a few locations near resonant orbits with Jupiter. Finally, it is also thought that meteorites sample the inner main belt [6], although it is possible that meteorites can be transported from further out [7]. The metamorphic evolution of asteroids is preserved within the meteorite collection and can give us information on differentiated asteroids such as in the case of Vesta with the HED group of meteorites [8].

Some good matches have been made between individual meteorite spectra and Near-Earth Asteroids (NEAs) [9] as well as between meteorite spectra and large main belt asteroids (MBAs) [10]. The principal properties of the spectra used to identify possible matches between meteorites and asteroids are the band minimum location and Band Area Ratio (BAR). The band minimum is the wavelength of an absorption band in the spectra. The BAR is the ratio between the area of the bands in the spectra. These properties are diagnostic of the object's mineralogy and, to a lesser extend, of other physical properties such as surface roughness and grain size [11]. The spectra of meteorites and asteroids are also dependent on observational conditions such as the phase angle between the line connecting the light source (e.g., the Sun) with the target and the line connecting the target with the observer. This is a key effect that needs to be understood to help improve matches between meteorites and asteroids, as this phase angle, when observing asteroids, varies due to the ever changing orbital positions of the viewer and the target. Variations in the band depths, band minimum locations, the band area ratio, and spectral slope have been noted to vary with phase angle and have been characterized [12]. Although this effect does not seem to affect the mineralogical analysis very much, it is important for understanding optical effects and their relationship to physical properties such as surface roughness and grain size.

When it comes to spectral modeling, Hapke's radiative transfer model has been utilized in most of the studies: S. J. Lawrence and P. G. Lucey used Hapke mixing models to model asteroid mineralogy [13], whereas B. E. Clark modeled S-type asteroid spectra [14]. In this study, we abandoned the Hapke model and utilized a ray-optics code that accounts for internal diffuse scatterers, to derive the refractive indices for both clinopyroxene and bronzite, and to further model the reflectance spectra of three meteorites. The corresponding measured meteorite reflectance spectra were obtained with the University of Helsinki integrating-sphere UV-Vis-NIR spectrometer. The details of the model are described in Section 4.1 and the modeling results are presented in Section 5.2.

2. Light scattering

2.1. Ray optics

The size of the particle can be described as a size parameter $x = ka$, where k is the wave number and a is the mean radius of the particle. In geometric optics, a Stokes parameter vector is related to every ray. At a boundary surface, refraction and reflection take place according to Snel's law and Fresnel's reflection and refraction matrices.

In the ray optics approximation [15]:

$$\sigma_{\text{ext}} = \sigma_{\text{abs}} + \sigma_{\text{sca}} \tag{1}$$

where σ_{ext} and σ_{abs} are extinction and absorption cross sections.

The single-scattering albedo $\tilde{\omega}$ is defined as [16]:

$$\tilde{\omega} = \frac{\sigma_{\text{sca}}}{\sigma_{\text{ext}}}. \tag{2}$$

The phase matrix P can be obtained from:

$$\mathbf{P} = \frac{4\pi}{k^2 \sigma_{\text{sca}}} S, \tag{3}$$

where S is the 4x4 element scattering matrix describing the scattering event in terms of angular dependence, and links the Stokes parameters of the incident and scattered fields [16]:

$$[I_{\text{sca}}, Q_{\text{sca}}, U_{\text{sca}}, V_{\text{sca}}]^T = \frac{1}{k^2 r^2} S [I_{\text{inc}}, Q_{\text{inc}}, U_{\text{inc}}, V_{\text{inc}}]^T. \tag{4}$$

The ray optics with diffuse and specular interactions (RODS) method, which uses the scattering phase matrix $\mathbf{P}$, single-scattering albedo $\tilde{\omega}$, and extinction mean free-path length l_0 to account for internal inhomogeneities, was utilized to model the reflectance spectra of meteorites. In this method, the diffuse scatterers are distributed inside an isotropic and homogenous medium that has a complex refractive index m. The extinction mean free-path length l_0, which describes the average distance traveled by the ray, can be obtained from [15]

$$l_o = \frac{1}{k_0}, \tag{5}$$

where k_0 is the extinction coefficient and can be written as

$$k_0 = n_0 q_{\text{ext}} \pi a^2 = \frac{3\nu_0 q_{\text{ext}}}{4a}, \tag{6}$$

where q_{ext} is the extinction efficiency, a is the mean radius of the particle, n_0 is the number density, and ν_0 is the volume density.

In geometric optics, there are no interference effect among the fields scattered by the particles in the system, and thus the scattered electromagnetic field can be considered incoherent. The incoherent scattered electromagnetic field $\mathbf{E}^s_{i,ic}$ is obtained by subtracting the coherent field $\mathbf{E}^s_c$ from the free-space scattered field of a specific volume element $\mathbf{E}^s_i$ [17], [18]:

$$\mathbf{E}^s_{i,ic} = \mathbf{E}^s_i - \mathbf{E}^s_c. \tag{7}$$

The coherent scattered electromagnetic field can be obtained by ensemble averaging the field scattered by individual realizations for finite volumes of spherical particles [19]:

$$\mathbf{E}^s_c = \frac{1}{N_r} \sum_{i=1}^{N_r} \mathbf{E}^s_i, \tag{8}$$

where N_r is the number of realizations. Geometric optics input is incoherent a priori and the scattering phase matrix $\mathbf{P}$ is computed using the incoherent scattering matrices.

For our spectral model, we combine olivine and pyroxene particles that contain microiron scatterers by averaging their single-scattering albedos $\tilde{\omega}$, mean free-path lengths l_o, and phase matrices $\mathbf{P}$. The averaged single-scattering albedo $\tilde{\omega}_{\text{avg}}$ is obtained by dividing the averaged scattering cross section $\sigma_{\text{sca,avg}}$ with the averaged extinction cross section $\sigma_{\text{ext,avg}}$:

$$\tilde{\omega}_{\text{avg}} = \frac{\sigma_{\text{sca,avg}}}{\sigma_{\text{ext,avg}}}. \tag{9}$$

The averaged scattering cross section is calculated by adding up scattering cross sections for olivine and pyroxene particles and weighting them based on their ratio in the meteorite. The averaged extinction cross section is calculated similarly using extinction cross sections of both olivine and pyroxene particles. The phase matrices are averaged by first averaging the scattering matrices using weights and then converting the averaged scattering matrix back to a phase matrix by utilizing the averaged scattering cross section in eq. (3). The averaged mean free-path length can be obtained from

$$l_0 = \frac{1}{\kappa_{\text{ext,tot}}}, \tag{10}$$

where $\kappa_{\text{ext,tot}}$ is a weighted sum of the averaged κ_{ext} for olivine and pyroxene particles. In a volume element δV, the ensemble average of total extinction cross section is $\langle \sigma^{\text{tot}}_{\text{ext}} \rangle$. In this

volume, the particles occupy an averaged volume $\langle V_{\rm ext}^{\rm tot}\rangle$. When the corresponding quantities for one particle are $\langle\sigma_{\rm ext}^{1}\rangle$ and $\langle V_{\rm ext}^{1}\rangle$, $\kappa_{\rm ext}$ can be obtained [20]:

$$\begin{aligned}
\kappa_{\rm ext} &= \frac{\langle\sigma_{\rm ext}^{\rm tot}\rangle}{\delta V} \\
&= \frac{\langle\sigma_{\rm ext}^{\rm tot}\rangle}{\langle V_{\rm ext}^{\rm tot}\rangle}\frac{\langle V_{\rm ext}^{\rm tot}\rangle}{\delta V} \\
&= \frac{\langle\sigma_{\rm ext}^{\rm tot}\rangle}{\langle V_{\rm ext}^{\rm tot}\rangle}\nu_0 \\
&= \nu_0\frac{\langle\sigma_{\rm ext}^{1}\rangle}{\langle V_{\rm ext}^{1}\rangle} \\
&= \nu_0\frac{3\langle\sigma_{\rm ext}^{1}\rangle}{4\pi a^3{\rm exp}(3\beta^2)} \\
&= 3\nu_0\frac{\langle\sigma_{\rm ext}^{1}\rangle}{4\pi a_{\rm vol}^3} \\
&= 3\nu_0\frac{\langle q_{\rm ext}^{1}\pi a_{\rm perp}^2\rangle}{4\pi a_{\rm vol}^3} \\
&= 3\nu_0\frac{\langle q_{\rm ext}^{1} a_{\rm perp}^2\rangle}{4\pi a_{\rm vol}^3},
\end{aligned} \tag{11}$$

where ν_0 is the volume density, β is the logradius standard deviation, $a_{\rm perp}$ is the average of the projected area, and $a_{\rm vol}$ is obtained from

$$a_{\rm vol} = a{\rm exp}({\rm log}(1+\sigma^2)) \tag{12}$$

where σ is the relative standard deviation for the radial distance.

2.2. Gaussian-random-sphere particles

Our ray-optics code simulates light scattering by Gaussian-random-sphere particles that are larger than the wavelength of the incident light. The Gaussian random particle is an infinite ensemble of sample particles that is obtained from its probability density function. Gaussian sphere $\mathbf{r} = r(\theta,\phi)\mathbf{e}_r$, which is described by spherical coordinates (θ,ϕ) by the spherical-harmonic series for the logarithmic radial distance $s = s(\theta,\phi)$, is [15]:

$$r(\theta,\phi)\mathbf{e}_r = \frac{a\exp[s(\theta,\phi)]}{\sqrt{1+\sigma^2}}\mathbf{e}_r,$$

$$s(\theta,\phi) = \sum_{l=0}^{\infty}\sum_{m=-l}^{l} s_{lm}Y_{lm}(\theta,\phi),$$

$$s_{l,-m} = (-1)^m s_{lm}^*, \tag{13}$$

where σ is the relative standard deviation for the radial distance and a is the mean radius, s_{lm}s are the Gaussian random variables with zero means, and Y_{lm}s are the orthonormal spherical harmonics.

Parameters describing the Gaussian random sphere are a and C_l, which relate to each other through [15]:

$$\sum_{l=0}^{\infty} C_l = \log_e(1+\sigma^2), \tag{14}$$

where $C_l \geq 0 \quad (l = 0, ..., \infty)$. By choosing the power-law covariance function, C_l can be further parameterized:

$$C_0 = C_1 = 0, \tag{15}$$

$$C_l = \frac{\widetilde{C}}{l^\nu}, l = 2, 3, ..., l_{\max}, \tag{16}$$

$$\widetilde{C}\sum_{l=2}^{l_{max}}\frac{1}{l^\nu} = \log_e(1+\sigma^2) \Rightarrow \widetilde{C} = \log_e(1+\sigma^2)\left[\sum_{l=2}^{l_{max}}\frac{1}{l^\nu}\right]^{-1}, \tag{17}$$

where $\widetilde{C}$ is a normalization constant, and the standard deviation σ and the power law index ν are statistical shape parameters.

The average volume depends on the logradius standard deviation β and the mean radius a [21]:

$$\langle V\rangle = \frac{4}{3}\pi a^3\exp(3\beta^2). \tag{18}$$

The detailed mathematical presentation for the shape of the Gaussian random sphere is described in [15].

3. Measurements

3.1. Experimental setup

The reflectance spectra were measured with the University of Helsinki integrating-sphere UV-Vis-NIR spectrometer [22], which has a quartz tungsten-halogen light source and a deuterium light source. The light is collimated using a rectangular slit and a circular aperture. Two different integrating spheres were used: a polytetrafluoroethylene (PTFE) coated integrating sphere for the UV-Vis wavelength region, and a gold coated integrating sphere for the NIR wavelength region. The measurements were carried out using a 2.5mm slit and a 2.5mm aperture. Before entering the integrating sphere, the collimated light goes through a grating mirror monochromator. The meteorite sample is placed on a Teflon sample holder, which reflects negligible amount of light at the measured wavelength range, and positioned in the integrating sphere so that the incident beam reflects from it. The angle between the incident beam and the normal vector of the sample holder is 10 degrees. There is a light trap at the mirror angle so that no specular reflection hits the detector.

The measurements were carried out using a wavelength range of 250 to 2500 nm with 5-nm sampling step. For each measurement sequence, the reflectance spectrum of the integrating sphere was measured first before measuring the spectrum of the meteorite sample. These reflectances were compared and corrected with the known calibrated values of the coating of the integrating sphere in order to get the meteorite sample's reflectance spectrum normalized against an ideal diffuser.

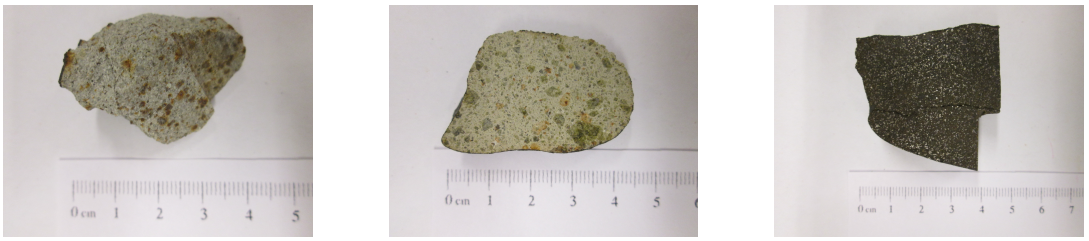

(a) Kisvarsany (L6) (b) Johnstown (diogenite) (c) St Germain du Pinel (H6)

Figure 1: Pictures of the measured meteorite pieces.

3.2. Meteorite samples

We measured the reflectance spectra of three meteorite pieces: Kisvarsany, Johnstown, and St. Germain du Pinel (see Fig.1) . The samples were borrowed from the Geological Museum of the Finnish Museum of Natural history. One sample is a diogenite, one is an H ordinary chondrite, and one is an L ordinary chondrite. All of the samples represent meteorite falls, i.e. they were collected after their fall in the atmosphere was observed. The measured surfaces were unpolished and contained no fusion crust on the measured surface.

4. Numerical methods

4.1. Spectral modeling with SIRIS4

The reflectance spectra of meteorites can be modeled by combining the most common materials (see Section 2.1) that dominate their spectral features, such as olivine, pyroxene, and iron. The spectral modeling was carried out for the Johnstown, St Germain du Pinel, and Kisvarsany meteorites. We utilized a new code, SIRIS4 [23], that is an updated version of the ray-optics code SIRIS [15], and takes into account the propagation of light as inhomogeneous plane waves inside absorbing particles. The first author of this paper updated the SIRIS4-code to account for diffuse scatterers that constitute an internal medium spanning uniformly across the particle interior. The spectral features were modeled by adding different amounts of microiron scatterers with a diameter of 6 micrometers inside a mixture containing different ratios of olivine and pyroxene. For the computations, we needed the complex refractive indices m of the materials as input parameters. The refractive indices for both olivine and iron were derived from [24], [25], and [26] (data retrieved from Jena Database of Optical Constants for Cosmic Dust and Refractiveindex.info, and further processed by A. Penttilä) (see Fig. 2 and Fig. 3). The real part of the refractive index for olivine does not change significantly at the modeled wavelength region, and was thus fixed to 1.6. The refractive indices for pyroxene (see Section 4.2) were obtained by utilizing an optimization code that uses SIRIS4.

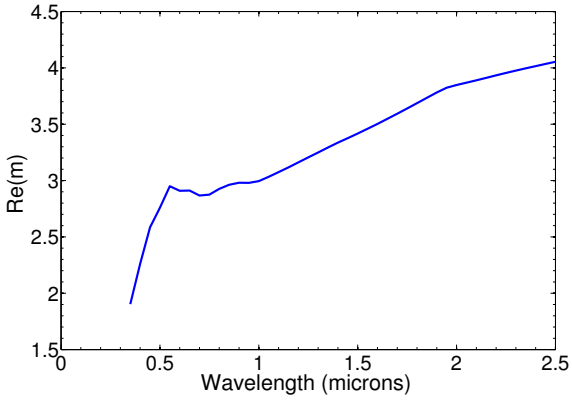

Figure 2: The real part of the refractive indices for iron.

First, the scattering matrices and single-scattering albedos for microiron particles in both olivine and pyroxene environment were computed using Gaussian-random-sphere particles in SIRIS4 with a wavelength range of 250 nm to 2500 nm. The obtained scattering phase matrices and single-scattering albedos were then utilized in SIRIS4 so that these microiron scatterers acted as diffuse scatterers inside olivine and pyroxene particles with a radius of 100 µm. The microiron scatterers were uniformly distributed inside both olivine and pyroxene particles, and the volume fraction used for microiron was different for each meteorite piece. The computed scattering matrices and single-scattering albedos for microiron in olivine

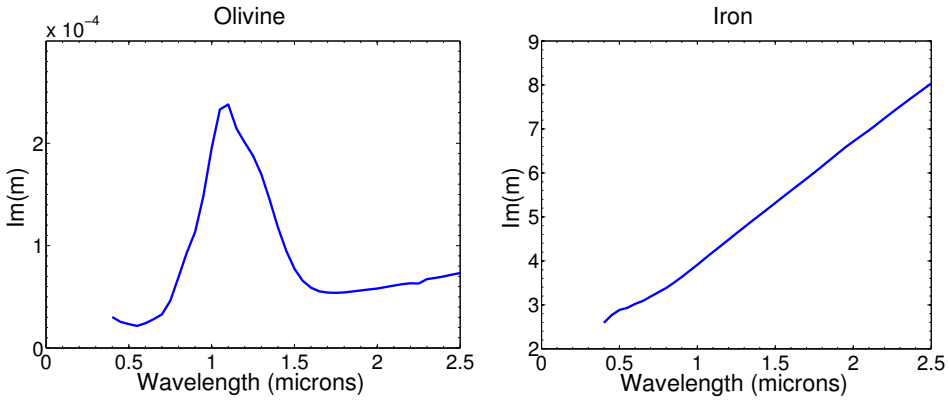

Figure 3: The imaginary parts of the refractive indices for olivine and iron.

and in pyroxene were then averaged using different ratios of olivine and pyroxene for each meteorite to get the best match between the measured and modeled specta. Finally, we carried out macroscopic mixing of minerals by averaging the computed scattering matrices and single-scattering albedos and then utilizing them in SIRIS4 so that the 100 µm averaged olivine and pyroxene particles with microiron scatterers acted as diffuse scatterers inside vacuum space of a radius of a few centimeters in order to model the whole meteorite piece. The volume fraction of the olivine and iron particles in the vacuum space was set to 0.3, however, changing this value does not affect the modeled spectra because the vacuum space does not absorb light, and thus the changes in the mean free-path length are irrelevant.

4.2. Derivation of the refractive indices

The imaginary parts of the refractive indices for pyroxene were derived by utilizing an optimization code written by the first author of this paper. The code uses the measured spectrum of the material and the SIRIS4 code. We obtained the measured reflectance spectra of clinopyroxene for different grain sizes [27]. In order to derive the refractive indices, we first set the upper and lower boundaries for the imaginary parts of the refractive indices. We fixed the real part of the refractive index to 1.8 at all wavelengths due to the fact that it does not significantly change at the modeled wavelength region [28] and thus does not have a remarkable effect on the modeled spectra. Bisection method was used to obtain Im(m) at a certain wavelength within the set upper and lower boundaries. The value was then entered as an input parameter into SIRIS4 to calculate the single-scattering albedo, which was then compared to the measured value of the reflectance spectrum at the same wavelength. The derived value for the Im(m) was iterated until the error between the derived single-scattering albedo value and the measured value of the spectrum was less than 0.001. The same procedure was carried out for the whole spectrum of clinopyroxene with a grain size of 44 microns. The optimization was run on a MATLAB pipeline that first read the measured reflectance spectrum values and upper and lower boundaries for Im(m) as input

parameters and then optimized Im(m) for each wavelength by using the bisection method and SIRIS4. The derived Im(m) (see Fig. 4) are over two times larger than those derived in [27] using the radiative transfer model of Hapke [29],[30] on the same measured spectrum. If the grain size was changed, the derived Im(m) in [27] also changed. To fix this, the grain sizes were optimized so that the deviation from the mean was minimized. In comparison, we utilized our Im(m) to model the reflectance spectra for clinopyroxene grains with a diameter of 12 and 94 µm (see Fig. 5). The resulting modeled spectra match well with the measured spectra, and thus the Im(m) can be used to model the clinopyroxene spectrum for any grain size.

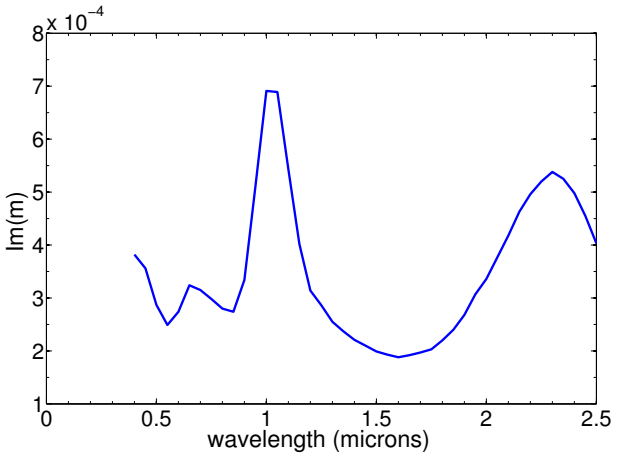

Figure 4: The imaginary part of the refractive index for clinopyroxene.

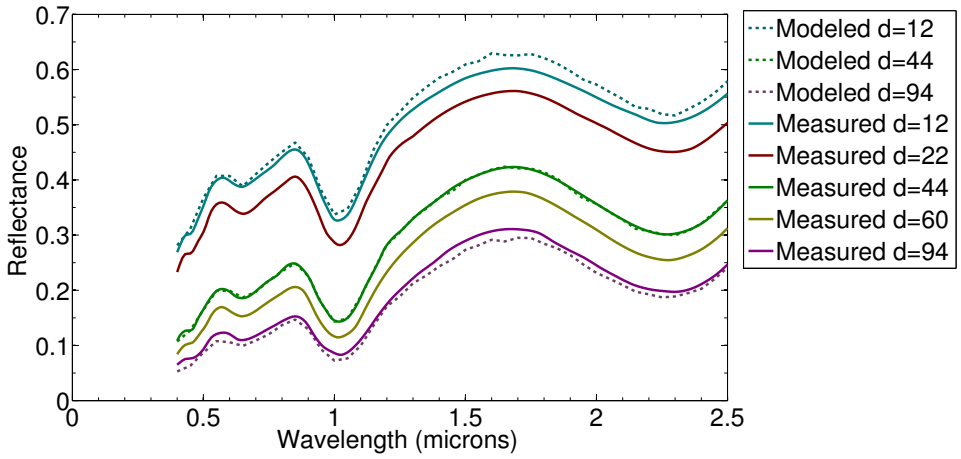

Figure 5: The measured and modeled spectra for clinopyroxene with varying grain sizes.

For our modeling purposes, we took the measured reflectance spectrum of bronzite min-

eral from the United States Geological Survey (USGS) Digital Spectral Library [31]. The Im(m) were derived as described above. The derived Im(m) and the modeled reflectance spectrum using the derived Im(m) and the measured reflectance spectrum of bronzite are shown in Fig. 6. It should be taken into consideration that comparing single-scattering albedo values and spectral reflectance values can cause some errors.

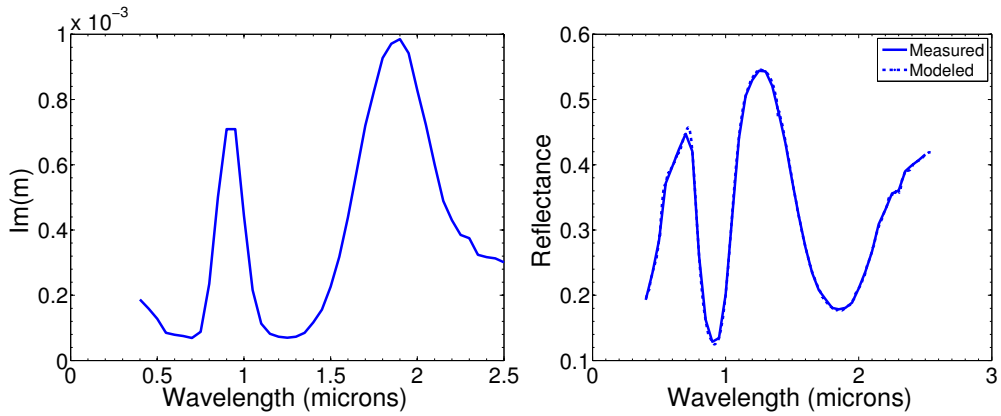

Figure 6: The imaginary part of the refractive index for bronzite and its measured and modeled spectra.

5. Results and Discussion

5.1. Spectral measurements

The measured reflectance spectra of the Johnstown, St Germain du Pinel, and Kisvarsany meteorites are shown in Fig. 7. In our integrating-sphere spectral measurements, the signal to noise ratio (S/N) varies with the three detectors that are used at different wavelengths. Roughly, the S/N is at the level of 100 for UV wavelengths, 5000 at visual wavelengths, and 500–1000 for NIR wavelengths. The St Germain du Pinel meteorite, which is classified as an H ordinary chondrite, and the Kisvarsany meteorite, which is classified as an L ordinary chondrite, have similar spectral features: a broad maximum in the spectrum at 0.7 µm, and an absorption feature near 0.9 µm. The reflectivity rises toward 1.5 µm, and a broad absorption band is centered at 1.9 µm. These characteristic spectral features are caused by olivine and pyroxene, the most abundant minerals in ordinary chondrites. There is also a small bump in the spectrum at about 1.3 µm caused by feldspar. The reflectance spectrum of the St Germain du Pinel meteorite is darker and flatter because H ordinary chondrites contain a high amount of iron.

The Johnstown meteorite is a diogenite (a type of achondritic stony meteorites), originating from asteroid (4) Vesta [32]. It does not contain olivine, so its spectrum is dominated by pyroxene. The spectrum rises deeply in the blue, has a deep absorption band centered at

0.9 µm, a maximum in reflectance at about 1.5 µm, and a broad absorption feature centered at 2.0 µm.

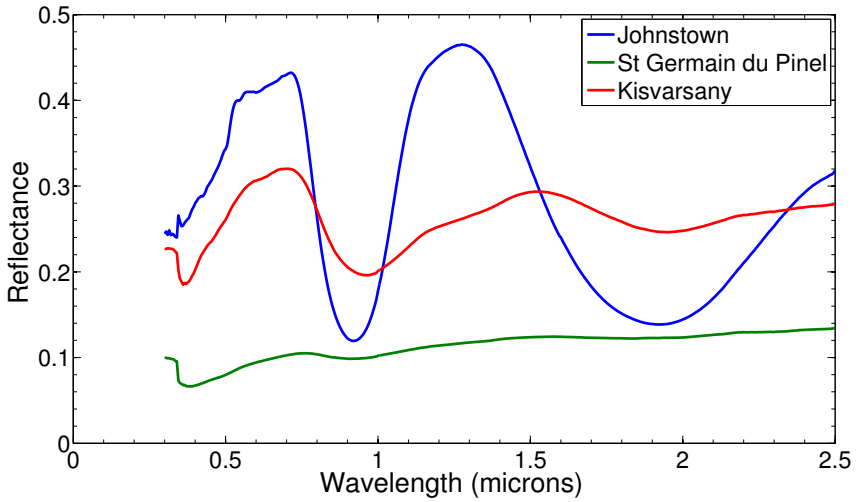

Figure 7: The measured reflectance spectra.

All measured reflectance spectra have a false through near 0.35 micrometers, which is caused by the spectrometer.

5.2. Spectral modeling

To model the measured reflectance spectra of the meteorites, the SIRIS4 light-scattering code was run for the wavelength range of 250 nm to 2500 nm with 50 nm steps. Each run lasted around 10 minutes and they were run in parallel. The number of rays used for one run was 100000 and the number of sample particles for a single run was 1000. Each computational step required a significant amount of data processing with MATLAB. The details of the computations can be found in Section 4.1.

The measured and modeled reflectance spectra for the meteorites are shown in Figs. 8 and 9, and the materials used in the models are shown in Table 1. The Johnstown meteorite was best modeled by using only the bronzite mineral. Adding microiron scatterers or olivine changed the spectra so that the modeled and measured spectra did not match. This result is consistent with the knowledge that the Johnstown meteorite does not contain olivine or microiron. The St Germain du Pinel meteorite was modeled by adding 4% microiron scatterers inside material that contained 65% olivine and 35% pyroxene. The Kisvarsany meteorite was modeled by adding 0.1% microiron scatterers inside material that contained 55% olivine and 45% pyroxene.

The small differences between the measured and modeled spectra can be caused by a) small amounts of other materials than olivine, pyroxene and iron in the meteorite, or b) slightly different type of olivine or pyroxene that was used in the model. The model that was used is still preliminary, and that can be seen in the results.

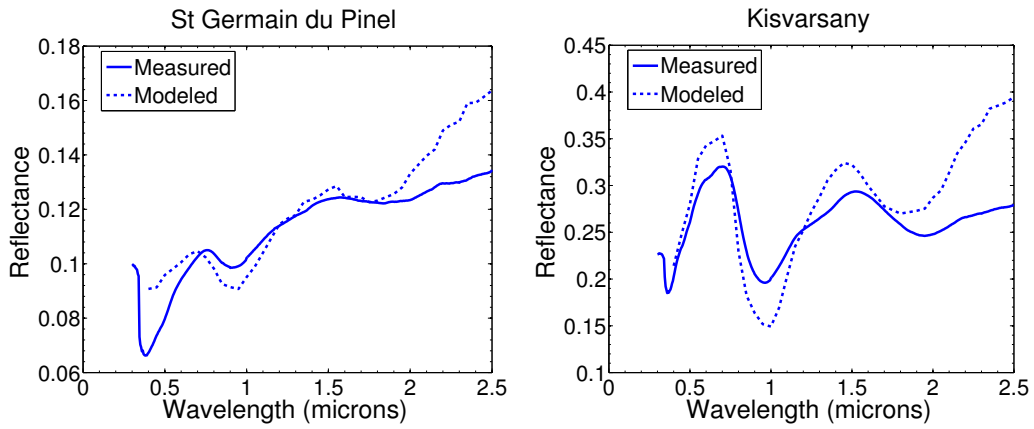

Figure 8: The measured and modeled spectra of the St Germain du Pinel and the Kisvarsany meteorites.

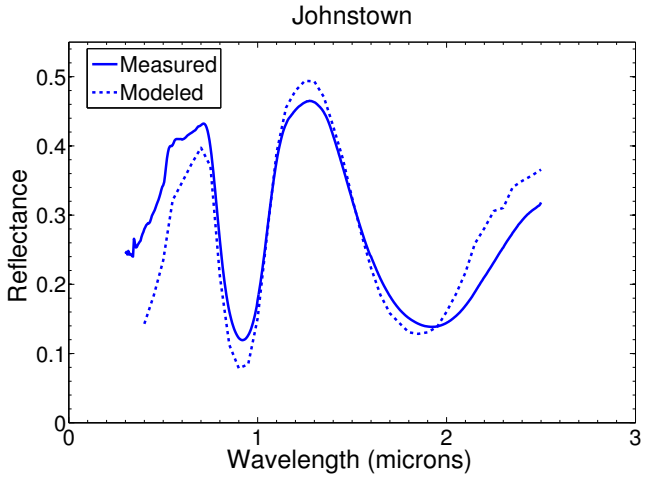

Figure 9: The measured and modeled spectra of the Johnstown meteorite.

Meteorite	Type	Materials used in the model
Johnstown	Diogenite	Pyroxene (bronzite)
St Germain du Pinel	H6	55% olivine, 45% pyroxene, 4% microiron
Kisvarsany	L6	65% olivine, 35% pyroxene, 0.1% microiron

Table 1: The materials used in the models.

5.3. Modeling the Gaussian-random-sphere particles

For this study, we examined how the shapes of the Gaussian-random-sphere particles affect the modeled spectrum of the Kisvarsany meteorite. In the first part, we modeled the spectra of the meteorite piece by setting the power law index to 2.5 and 3.5. In the second part, the spectra of the meteorite piece were modeled by setting the standard deviation of the radial distance to 0.12 and 0.22. The mean radius used for the Gaussian random sphere was obtained by utilizing eq. (18) and setting the volume of the Gaussian random sphere equal to the volume of the Gaussian random sphere with a standard deviation of 0.17. Finally, the computed meteorite spectra were compared with the modeled spectrum of the Kisvarsany meteorite with power law index 3 and standard deviation 0.17 (see Fig. 10). Fig. 11 shows illustrations of the different shapes.

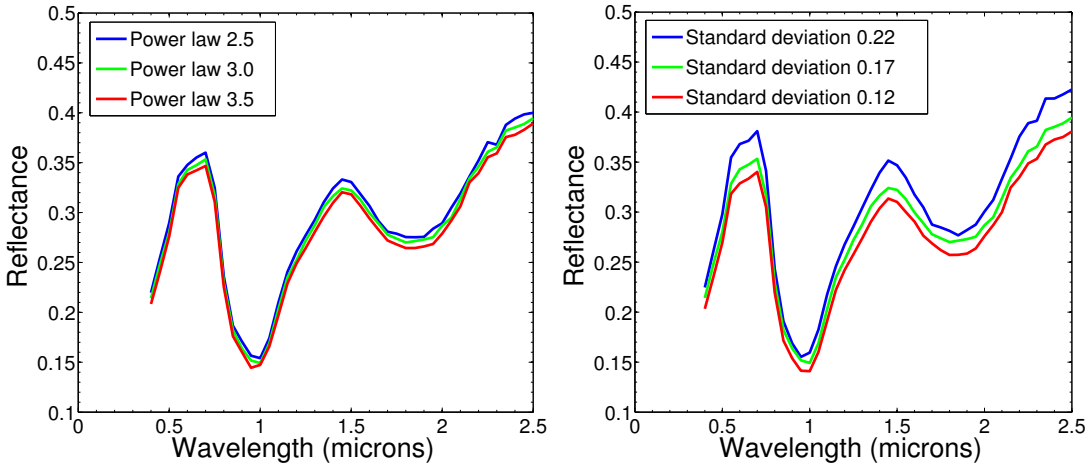

Figure 10: The modeled specta of the Kisvarsany meteorite with different power law index values and standard deviations.

Changing the value of the power law index does not affect the reflectance significantly. However, the standard deviation has a more notable effect on the spectral shape. Increasing the standard deviation also increases the reflectance. The largest differences can be seen at the reflectance peaks near 0.7 µm and 1.5 µm, and at the longer wavelengths. This

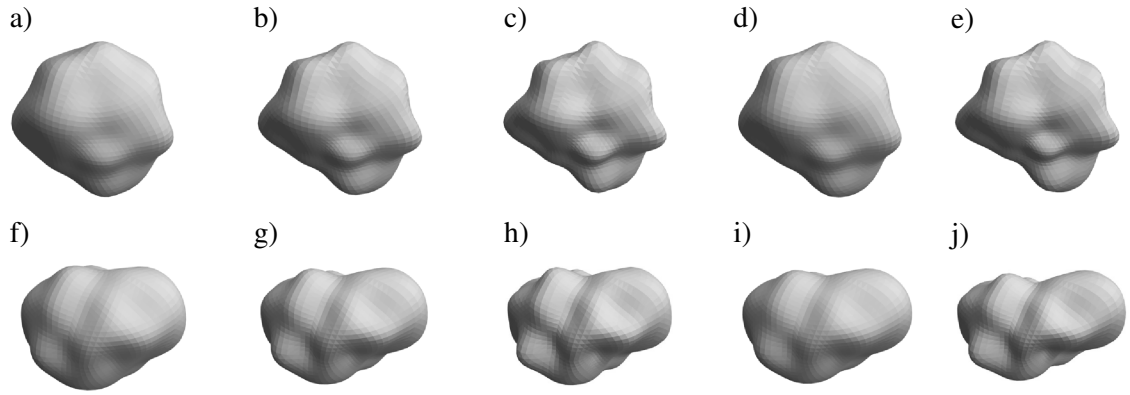

Figure 11: The modeled Gaussian-random-sphere particles: a) and f) are with $\sigma = 0.17$ and $\nu = 2.5$, b) and g) are with $\sigma = 0.17$ and $\nu = 3.0$, c) and h) are with $\sigma = 0.17$ and $\nu = 3.5$, d) and i) are with $\sigma = 0.12$ and $\nu = 3.0$, e) and j) are with σ 0.22 and $\nu = 3.0$. The sequence of the random numbers used in creating the shapes is starting with a seed of 1 for the first row, and with a seed of 2 for the second row of shapes.

implies, that in order to carry out accurate spectral modeling, we would need to utilize a true geometric model of the sample meteorite.

6. Conclusions

The aim of our research was to model the measured reflectance spectra of the Kisvarsany, Johnstown, and St Germain du Pinel meteorites using a ray-optics code that accounts for inhomogeneous waves and internal diffuse scatterers. This study was carried out in multiple parts. First, the SIRIS4 light-scattering code was updated so that it takes internal diffuse scatterers into account. Second, the reflectance spectra of the meteorites were measured with the University of Helsinki UV-Vis-NIR integrating-sphere spectrometer. All meteorite samples were "falls" derived from original specimens of a few centimeters in size. The measured areas of the samples were unpolished and free of fusion crust. Third, the refractive indices for pyroxene were derived by utilizing an optimization code that uses the measured spectrum of the material and the SIRIS4 code. After obtaining the complex refractive indices for olivine, iron and pyroxene, spectral modeling was carried out for the three meteorite pieces. Finally, a spectral modeling was carried out for the Kisvarsany meteorite using different values for standard deviation and power law index to study how the shapes of the Gaussian-random-sphere particles affect the resulting modeled spectra.

The reflectance spectra of the three meteorite pieces could be modeled quite accurately by using only olivine, pyroxene, and iron in the models. The differences between the measured and modeled spectra were most likely caused by small amounts of other materials than olivine, pyroxene and iron in the meteorite, or a different type of olivine or pyroxene, that were not taken into account in the computations. After computing the scattering matrices and single-scattering albedos for olivine and pyroxene particles containing microiron scatterers, we used macroscopic mixing of minerals that can be the cause of some of the differences between the measured and modeled spectra.

We showed, that when modeling Gaussian-random-sphere particles, changing the value for the power law index does not have a significant impact on the modeled spectra. However, changing the value for the standard deviation had a larger effect on the spectra, that could be clearly seen at the reflectance peaks near 0.7 µm and 1.5 µm, and at the longer wavelengths.

In the future, the meteorite reflectance spectra can be modeled more accurately by improving the model and trying out different materials that are abundant in meteorites. Applicability of our spectral model can also be extended to asteroid spectra.

Acknowledgements

The research was funded by the SAEMPL ERC Advanced Grant No. 320773. H. Lindqvist acknowledges funding from the Academy of Finland via project number 285421. We would like to thank Arto Luttinen from the Finnish Museum of Natural History for letting us borrow the meteorite samples.

References

[1] P. A. Bland, T. B. Smith, A. J. T. Jull, F. J. Berry, A. W. R. Bevan, S. Cloudt, C. T. Phillinger, The flux of meteorites to the earth over the last 50,000 years, Monthly Notices of the Royal Astronomical Society 283 (1996) 551–565.

[2] M. I. Gritsevich, V. P. Stulov, L. I. Turchak, Consequences for collisions of natural cosmic bodies with the earth atmosphere and surface, Cosmic Research 50 (2012) 56–64.

[3] O. Wilkman, M. Gritsevich, N. Zubko, J. Peltoniemi, K. Muinonen, Photometric modelling for laboratory measurements of dark volcanic sand, Journal of Quantitative Spectroscopy and Radiative Transfer 185 (2016) 37–47.

[4] Z. Ceplecha, P. Spurný, J. Borovička, J. Keclikova, Atmospheric fragmentation of meteoroids, Astronomy and Astrophysics 279 (1993) 615–626.

[5] P. Vernazza, R. P. Binzel, C. A. Thomas, F. E. DeMeo, S. J. Bus, A. S. Rivkin, A. T. Tokunaga, Compositional differences between meteorites and near-earth asteroids, Nature 454 (2008) 858–860.

[6] W. F. J. Bottke, D. Vokrouhlický, D. P. Rubincam, M. Brož, The effect of yarkovsky thermal forces on the dynamical evolution of asteroids and meteoroids, Asteroids III (2002) 395–408.

[7] D. Nesvorný, D. Vokrouhlický, A. Morbidelli, W. F. Bottke, Asteroidal source of l chondrite meteorites, Icarus 200 (2009) 698–701.

[8] T. B. McCord, J. B. Adams, T. V. Johnson, Asteroid vesta: spectral reflectivity and compositional implications, Science 168 (1970) 1445–1447.

[9] L. A. McFadden, M. J. Gaffey, T. B. McCord, Near-earth asteroids: possible sources from reflectance spectroscopy, Science 229 (1985) 160–163.

[10] R. P. Binzel, S. Xu, Chips off of asteroid 4 vesta: evidence for the parent body of basaltic achondrite meteorites, Science 260 (1993) 186–191.

[11] M. D. Paton, K. Muinonen, L. J. Pesonen, V. Kuosmanen, T. Kohout, J. Laitinen, M. Lehtinen, A pca study to determine how features in meteorite reflectance spectra vary with the samples' physical properties, Journal of Quantitative Spectroscopy and Radiative Transfer 112 (2011) 1804–1814.

[12] J. A. Sanchez, V. Reddy, A. Nathues, E. A. Cloutis, P. Mann, H. Hiesinger, Phase red- dening on near-earth asteroids: implications for mineralogical analysis, space weathering and taxonomic classification, Icarus 220 (2012) 36–50.

[13] S. J. Lawrence, P. G. Lucey, Asteroid Modal Mineralogy Using Hapke Mixing Models: Validation with HED Meteorites, Vol. 35, Lunar and Planetary Science Conference, 2004.

[14] B. E. Clark, Spectral mixing models of s-type asteroids, Journal of Geophysical Research 100 (1995) 443–456.

[15] K. Muinonen, T. Nousiainen, H. Lindqvist, O. Munoz, G. Videen, Light scattering by gaussian particles with internal inclusions and roughened surfaces using ray optics, Journal of Quantitative Spectroscopy and Radiative Transfer 110 (2009) 1628–1639.
[16] C. Bohren, D. Huffman, Absorption and scattering of light by small particles, Wiley-VHC, 1998.
[17] K. Muinonen, J. Markkanen, A. Virkki, A. Penttilä, D. Mackowski, Multiple scattering by dense random media: Volume-element extinction, 2016 URSI International Symposium on Electromagnetic Theory (EMTS).
[18] K. Muinonen, J. Markkanen, T. Väisänen, J. I. Peltoniemi, A. Penttilä, Multiple scattering in discrete random media using first-order incoherent interactions, Radio Science, Submitted, 2017.
[19] L. M. Zurk, L. Tsang, K. H. Ding, D. P. Winebrenner, Monte carlo simulations of the extinction rate of densely packed spheres with clustered and nonclustered geometries, J. Opt. Soc. Am. A 12 (1995) 1772–1781.
[20] J. Hansen, L. D. Travis, Light scattering in planetary atmospheres, Space Sci Rev 16 (1974) 527–610.
[21] K. Muinonen, Introducing the gaussian shape hypothesis for asteroids and comets, Astronomy and Astrophysics 332 (1998) 1087–1098.
[22] A. Penttilä, J. Martikainen, M. Gritsevich, K. Muinonen, Laboratory spectrometry of meteorites with an integrating-sphere at UV-Vis-NIR wavelengths, In preparation, 2017.
[23] H. Lindqvist, J. Martikainen, J. Räbinä, A. Penttilä, K. Muinonen, Ray optics with inhomogeneous waves applied to scattering by ice crystals, Journal of Quantitative Spectroscopy and Radiative Transfer, In preparation, 2017.
[24] D. Fabian, T. Henning, C. Jger, H. Mutschke, J. Dorschner, O. Werhan, Steps toward interstellar silicate mineralogy vi. dependence of crystalline olivine ir spectra on iron content and particle shape, Astronomy and Astrophysics 378 (2001) 228–238.
[25] P. B. Johnson, R. W. Christy, Optical constants of transition metals: Ti, v, cr, mn, fe, co, ni, and pd, Physical Review B 9 (1974) 5056–5070.
[26] M. A. Ordal, R. J. Bell, R. W. Alexander, L. A. Newquist, M. R. Querry, Optical properties of al, fe, ti, ta, w, and mo at submillimeter wavelengths, Appl. Opt. 27 (1988) 1203–1209.
[27] P. G. Lucey, Model near-infrared optical constants of olivine and pyroxene as a function of iron content, Journal of Geophysical Research 103 (1998) 1703–1713.
[28] A. Scott, W. W. Duley, Ultraviolet and infrared indices of amorphous silicates, The Astrophysical Journal 105 (1996) 401–405.
[29] B. Hapke, Bidirectional spectroscopy, 1, theory, Journal of Geophysical Research 86 (1981) 3039–3054.
[30] B. Hapke, Theory of Reflectance and Emittance Spectroscopy, Cambridge University Press, 1993.
[31] R. Clark, G. Swayze, R. Wise, K. Livo, T. Hoefen, R. Kokaly, Usgs digital spectral library splib06a, Vol. 231, U.S. Geological Survey Data Series, 2007.
[32] K. Donaldson Hanna, A. L. Sprague, Vesta and the hed meteorites: Mid-infrared modeling of minerals and their abundances, Meteoritics and Planetary Science 44 (2009) 1755–1770.